PLANETARY VOLCANIC PROCESSES: VAPOR PHASE TRANSPORT IN TERRESTRIAL AND LUNAR PYROCLASTIC DEPOSITS;

J.J. Papike, C.K. Shearer, M.N. Spilde, Institute of Meteoritics, Department of Geology, University of New Mexico, Albuquerque, NM 87131

Our group has initiated a study of vapor phase transport in terrestrial and lunar pyroclastic deposits. Recent studies of active terrestrial fumaroles [e.g.1] document very large vapor/melt partitioning as evidenced by study of condensate and sublimate accumulations. Volcanic gases from the andesitic Merapi Volcano, Indonesia [1] are enriched by factors greater than 10^5 in Se, Re, Bi and Cd; 10^4-10^5 in Au, Br, In, Pb, and W; 10^3-10^4 in Mo, Cl, Cs, S, Sn and Ag; 10^2-10^3 in As, Zn, F, and Rb; and 1-10^2 in Cu, K, Na, Sb, Ni, Ga, V, Fe, Mn, and Li. Several of the enrichment factors for sublimates studied by [1] are illustrated in figure 1.

Figure 1.

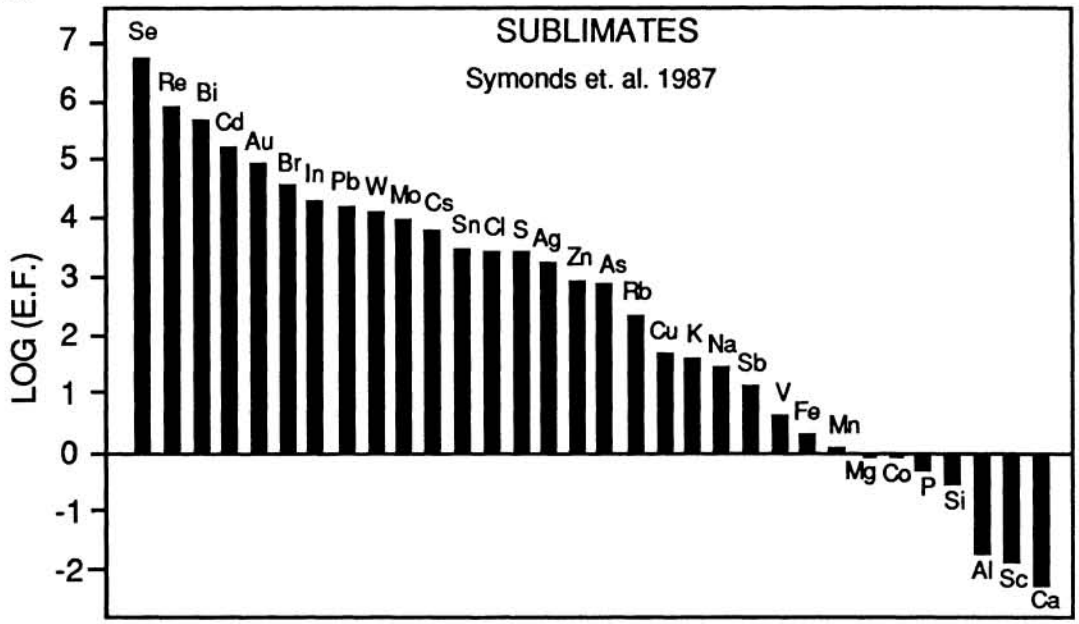

We are studying fossil fumarole deposits in the Valley of Ten Thousand Smokes(VTTS), Katmai, Alaska in andesite, dacitic, and rhyolitic pyroclastic deposits. Some representative trace element enrichment factors are listed in table 1 and figure 2. Thus it is clear that vapor transport is an extremely efficient transport mechanism in terrestrial volcanism. The vapor phase in terrestrial volcanic gases is composed of: H_2O, CO_2, SO_2, H_2, H_2S, HCL, CO, HF and S_2 [2,3]. In contrast, lunar volcanic gases are dominated by CO/CO_2 mixtures [4]or some combination of C-O-S [5]. Other species present in these gases include B, N, F, Na, S, Cl, Ar, Cu, Zn, Ga, Ge, Se, Br, Ag, Cd, In, Sb, Au, Hg, Tl, Pb, and Bi [6]. Numerous studies have documented that volatile elements such as S, Zn, Na, and the halogens are anomalously enriched on surfaces of the type-examples of lunar volcanic glass i.e. Apollo 15 green and Apollo 17 orange. It is evident that although terrestrial and lunar volcanic gases differ significantly in composition (H_2O vs CO/CO_2 dominated) both experienced efficient vapor/melt partitioning. We have initiated a SIMS study of volcanic glass beads [6] to see if the mantle reservoirs of the diverse glass bead types have different volatile budgets. Our preliminary work [7] on volcanic glass beads from Apollo 14 show that high-Ti (black and orange) beads have elevated concentrations of Zn and Cu. Note table 2 for selected SIMS data. Apollo 17 orange glass also has high Zn and Cu [8]. Apparently, high-Ti melts were associated with relatively high Zn and Cu mantle reservoirs under both the eastern and western Apollo sites. We plan to continue to access the volatile trace element characteristics of the different volcanic bead groups identified by Delano and co-workers with SIMS/PIXE techniques.

We [e.g. Shearer and Papike, this volume] and others have noted that picritic volcanic bead compositions are not easily related to mare basalt compositions by liquid line of descent trajectories. Can it be that these volcanic bead populations sampled mantle reservoirs anomalously enriched in volatiles which gave rise to the more energetic volcanic eruptive mechanisms (fire fountaining) of the beads then the mare basalts?

TABLE 1: MAXIMUM ENRICHMENT FACTORS IN VTTS FUMAROLES

	RHYOLITE PROTOLITH		DACITE PROTOLITH	
	63	64	Ash-Flow	Ash-Fall
Br	8.3	1.9	10.2	48.9
As	6.4	1.4	16.3	104.3
Zn	29.2	16.5	2.4	23.5
Pb	21.1	1.1	3.4	123.8
Sb	2.3	1.1	66.7	20.7
Cr	30.2	17.0	1.6	2.0
Cu	37.1	6.0	3.0	43.5
Au	18.0	33.1	3.3	13.3
Sn	46.0	1.0	1.6	14.0
Sr	6.4	25.2	1.1	1.4
V	166.0	55.2	1.3	2.3

TABLE 2: AVERAGE CHEMICAL COMPOSITION OF APOLLO 14 VOLCANIC BEAD GROUPS (ppm)

	Blk	Orng	VLT	Gr A	Gr B	Ylw	LAP
Li	19	14	7.7	7	n.a.	n.a.	8.4
Sc	40	40	39	40	31	43	44
V	170	150	160	150	110	81	111
Co	60	50	80	100	60	57	48
Cu	600	500	15	35	n.a.	n.a.	76
Zn	500	700	45	70	n.a.	n.a.	69
Rb	2	0.9	0.6	1.0	n.a.	n.a.	1.1
Sr	240	260	51	66	17	166	128
Y	80	98	41	41	n.a.	n.a.	64
Zr	500	480	210	200	60	255	345
Ba	400	400	140	200	40	138	240

The heterogeneous mantle reservoirs may have resulted from convective overturn of gravitationally unstable cumulates [e.g.9]. For example late cumulates enriched in Ti and P (Phosphates) could couple high densities with phosphate mineral volatile traps containing species such as F, Cl, CO_3 groups etc. which on melting in the deep mantle producing volatile enriched melts. These melts on ascent and during degassing result in volatile enriched pyroclastic deposits as represented in the glass bead population.

References: [1] Symonds et. al. (1987), G.C.A., 51, 2083-2101. [2] Greenland (1984) G.C.A., 48, 193-195. [3] Gerlach (1980) J. Volcanol. Geotherm. Res., 7, 295-317. [4] Basaltic Volcanism Study Project (1981) p. 394. [5] Grove (1981) Proc. 12 LPSC, Part B, 935-948. [6] Delano (1986), J.G.R., Proc. 16th LPSC, Part 2, D201-D213. [7] Papike, Shearer, Galbreath (1990) Geology, 18, 295-298. [8 Meyer et.al. (1975) Proc. 6th Lunar Sci. Conf. 1673-1699. [9] Spera (1990) Abstracts for workshop on Mare Volcanism and Basalt Petrogenesis. Lunar and Planetary Inst., Houston, 47-50.

Figure 2. Enrichment/depletion factors for dacite protolith (VTTS). Values to the left of vertical dashed lines represent overlying fall deposits; those to the right underlying flow deposits.

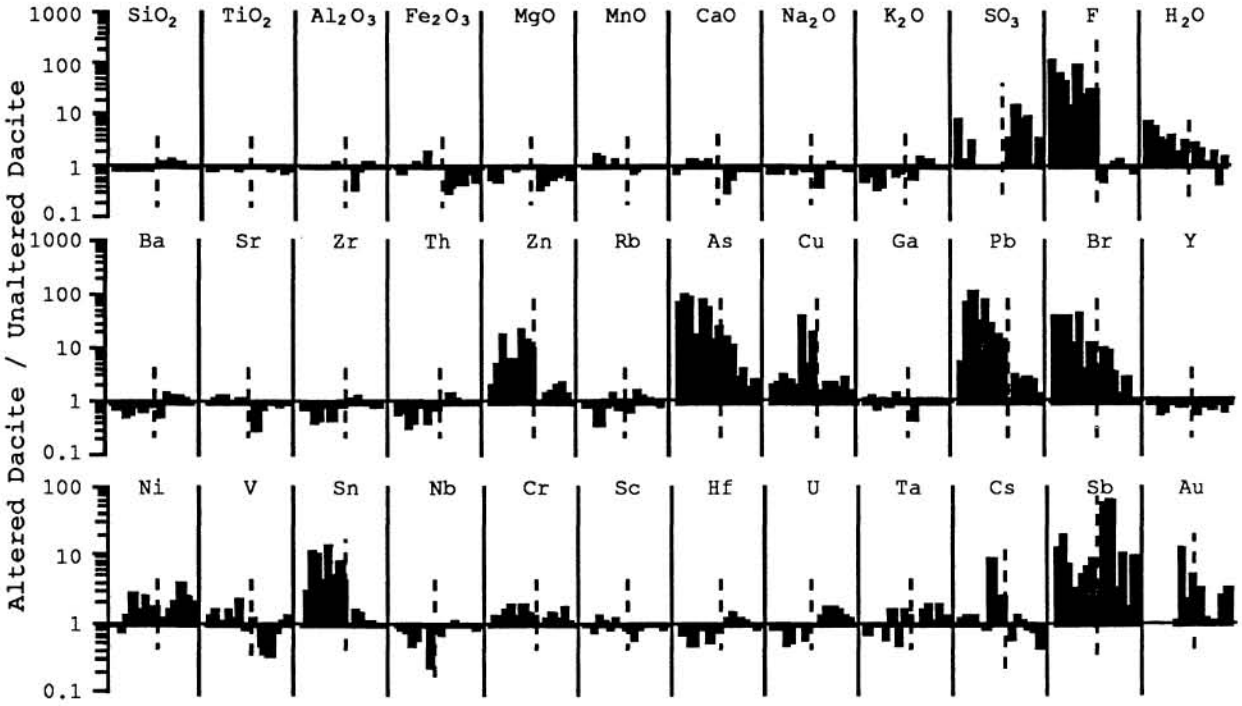

THE STRENGTH OF MIRANDA'S LITHOSPHERE; ***Robert Pappalardo and Ronald Greeley, Department of Geology, Arizona State University, Tempe, Arizona 85287***

In attempting to understand the endogenic processes which have shaped the surface of an icy satellite, it is desirable to quantify the failure strength of the satellite's lithosphere. In a crust that is fractured on a large scale, frictional sliding along pre-existing fractures occurs in response to lower differential stresses than required to initiate fracture of pristine rock, thus governing failure of a brittle lithosphere. Failure is predicted along favorably-oriented fracture planes; if fractures of all orientations are assumed to be present in the crust (as is expected of a heavily cratered lithosphere), frictional failure relations are directly applicable. The Coulomb criterion predicts that the shear stress σ_τ and normal stress σ_n components on a fracture plane at failure are related as $\sigma_t = \mu\sigma_n + S_o$ where S_o is the cohesion and μ is the coefficient of friction. At moderate to high pressures, the frictional sliding strength of most materials is found to be $\sigma_\tau = 0.85\sigma_n$ [1]. This strength is largely independent of rock type and strength, strain rate, and temperature.

The frictional failure curve for ice, however, deviates from this law [2]. At low temperatures ($77 \leq T \leq 115$ K) and moderate pressures ($\sigma_n < 200$ bar), ice frictional failure can be described by $\sigma_\tau = 0.55\sigma_n + 10$ bar, independent of temperature or sliding rate. The frictional failure curve for real surfaces probably does not have a cohesion intercept, but may instead have vertical tangency to the shear stress axis, conceptually intercepting the origin [3]. Constraining the frictional failure line for ice to pass through the origin, $\sigma_\tau = 0.69\sigma_n$ is obtained [2].

At low confining pressures ($\sigma_3 \lesssim 30$ bar), frictional sliding of a variety of rock types is strongly dependent on the surface roughness of the pre-existing fractures [1, 3]. Such low stresses are applicable in considering frictional failure of low gravity satellites such as Miranda. The frictional strength of ice has been tested down to $\sigma_3 = 3$ bar [2], but the effect of surface roughness has not been directly evaluated.

Near the horizontal surface of a planet, lithospheric stresses may be resolved into three principal stress directions, one of which is vertical and the other two are horizontal. In a lithosphere of average density ρ subject to gravitational acceleration g, the vertical principal stress can be equated (in the absence of pore pressure) to the lithostatic pressure ρgz at some depth z. In the case of horizontal compression, the maximum compressional stress σ_1 is horizontal and the minimum compressional (maximum tensional) stress σ_3 is vertical; in the case of horizontal extension, the opposite is true. With one principal stress thus known, the other necessary to induce failure may be determined by

$$\frac{\sigma_1}{\sigma_3} = 2\mu\left[\sqrt{\mu^2+1}+\mu\right]+1$$

for some value of friction and negligible cohesion [4].

The maximum horizontal stress that may be supported in a lithosphere may be represented as the difference $\sigma_H - \sigma_V$ between the horizontal and vertical principal stresses [5], with compression being considered positive. Frictional failure stress is plotted a function of depth in Figure 1 for a crustal density of 1000 kg m^{-3}, gravity $\approx$ 0.09 m s^{-2}, and friction values μ = 0.5 and 0.7, chosen as bounds to the ice frictional failure data.

As illustrated by Figure 1, frictional failure strength of the brittle lithosphere increases with depth as lithostatic pressure increases for both compression (σ_3 vertical, positive stress) and extension (σ_1 vertical, negative stress) until the brittle-ductile transition depth is reached. Below this depth, lithospheric strength is controlled by creep of the ductile crust and decreases with depth. Behavior of the ductile lithosphere is dependent upon composition, temperature, and strain rate. Plotted on Figure 1 are curves that represent the ductile strength of cold ice based on the data of [6]. A strain rate of 10^{-16} s^{-1} and a surface temperature of 60 K are chosen, and the labeled curves represent thermal gradients of 2, 5, 10, and 20 K km^{-1}.

The plot shows that the maximum strength of Miranda's lithosphere (that at the brittle-ductile transition) is small. Failure in compression (reverse faulting) is induced by $\lesssim$ 50 bar of horizontal stress, a stress close to that which may cause folding of an ice crust [7], indicating that both deformation styles might be active in a compressional regime. Less than 20 bar could cause failure in extension (normal faulting), a stress which could be supplied by satellite expansion of $\lesssim$ 0.05% [8].

If troughs in Miranda's Elsinore Corona are graben whose faults intersected near the brittle-ductile depth transition at the time of their formation, a transition depth of ~5 to 10 km is implied [9]. This necessitates a paleo-thermal gradient ~10 to 20 K km^{-1}. A steeper thermal gradient (and/or a lesser strain rate) is

STRENGTH OF MIRANDA'S LITHOSPHERE: ***R. Pappalardo and R. Greeley***

suggested if narrow troughs (~1 km wide) in Elsinore and Inverness Coronae are graben that formed in a similar fashion. A lower thermal gradient earlier in Miranda's history may have facilitated formation of broader troughs, which appear to be more ancient [10].

Comparing the results of Figure 1 to those for Ganymede [2], it is apparent that lower satellite gravity results in much lower frictional strength and in a somewhat deeper brittle lithosphere. Lower surface temperature significantly lowers the depth to ductile ice behavior for a given lithospheric stress, thermal gradient, and strain rate. The results here can be directly applied to Enceladus, which has a gravity and a surface temperature similar to those of Miranda. Enceladus displays subparallel troughs ~4 km wide that may be graben which formed in a brittle lithosphere ~3 km deep. For a water ice lithosphere, low stress but high paleo-thermal gradient (>20 K km^{-1}) is indicated. Such a high gradient is likewise necessary to account for the shapes of some craters on Enceladus if a water ice lithosphere is assumed [11].

The results of Figure 1 are somewhat suspect because of poor constraints on the creep of ice at very low temperatures. In addition, the lithospheres of Miranda and Enceladus are probably not composed of pure water ice: Miranda possesses a dark contaminant, and both lithospheres may be composed of a mixture of water and other ices, which could allow ductile behavior at lower temperatures and more gentle thermal gradients. In addition, the possible effect of fracture roughness needs to be evaluated, as this might cause the friction coefficient μ to vary be more than an order of magnitude, greatly affecting the slope of the frictional strength line.

The low frictional strength of low-gravity satellites permits relatively minor lithospheric stress to result in surface deformation; therefore, only small horizontal stresses are necessary to account for observed endogenic deformation on Miranda and Enceladus. The low surface temperature of these satellites necessitates steep thermal gradients to produce shallow ductile behavior of a water ice lithosphere.

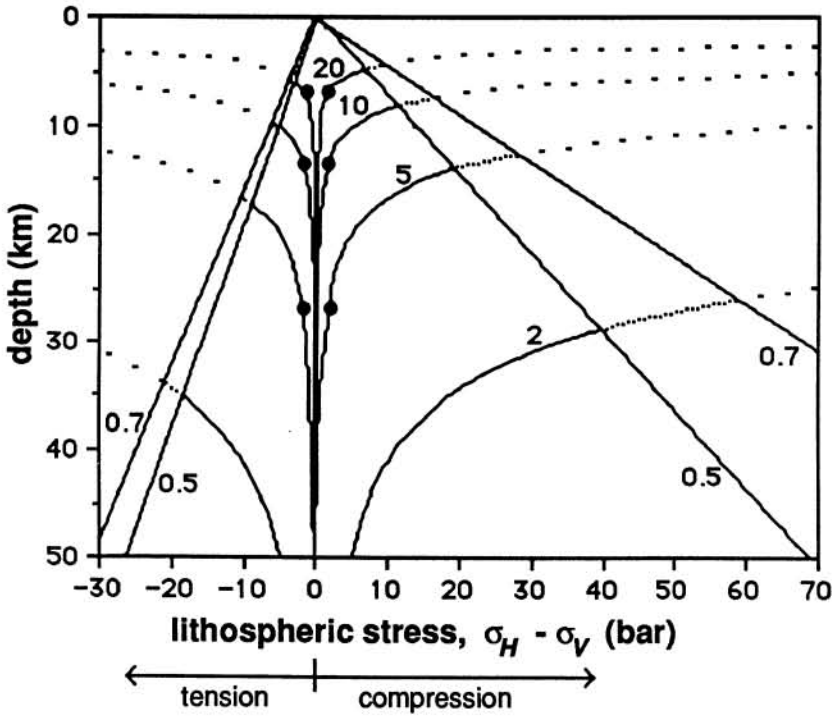

Figure 1. Maximum horizontal stress which can be supported in an ice lithosphere for Miranda (or Enceladus). Strength of the brittle lithosphere is controlled by frictional failure and is bracketed by straight lines for $\mu = 0.5$ and 0.7 for gravity $g \approx 0.09$ m s^{-2}. Ductile strength curves for cold ice are for a strain rate of 10^{-16} s^{-1}, a surface temperature of 60 K, and thermal gradients as indicated. Dots indicate depths at which T = 195 K is attained, below which the low-temperature ice flow law parameters used here are no longer strictly valid [6]. Compressional stress is taken to be positive.

[1]Byerlee, J.D., *Pure Appl. Geophys., 116*, 615, 1978. [2]Beeman, M. *et al., JGR, 93*, 7625, 1988. [3]Barton, N., *Int. J. Rock Mech. Min. Sci. Geomech. Abstr., 13*, 255, 1976. [4]Jaeger, J.C. and N.G.W. Cook, *Fundamentals of Rock Mechanics*, 1979. [5]Brace, W.F. and D.L. Kohlstedt, *JGR, 85*, 6248, 1980. [6]Kirby, S.H. *et al., J. Physique, 48, suppl.*, 227, 1987; Durham, W.B. *et al., JGR, 88*, B377, 1983. [7]Pappalardo, R. and R. Greeley, *in prep.* [8]Consolmagno, G.J., *Icarus, 64*, 401, 1985. [9]Pappalardo, R. and R. Greeley, *BAAS, 22*, 1057, 1990. [10]Croft, S.K., submitted to *Icarus*. [11]Passey, Q.R., *Icarus, 53*, 105, 1983.